


Equilibrium temperatures of discrete nonlinear systems

Uri Levy* and Yaron Silberberg

Weizmann Institute of Science, Rehovot 7610001, Israel

 (Received 4 June 2018; revised manuscript received 8 August 2018; published 30 August 2018)

During the evolution of discrete nonlinear systems with dynamics dictated by the discrete nonlinear Schrödinger equation, two quantities are conserved: system energy (Hamiltonian) and system density (number of particles). It is then possible to analyze system evolution in relation to an energy-density phase diagram. Previous works have identified a “thermalization zone” on the phase diagram where regular statistical mechanics methods apply. Based on these statistical mechanics methods we have now assigned a specific equilibrium temperature to every point of the thermalization zone. Temperatures were derived in the grand canonical picture through an entropy-temperature relation, modified to suit the nonlinear lattice systems. Generally, everywhere in the thermalization zone of the phase diagram, temperatures along a fixed system-density line, grow monotonously from zero to infinity. Isotherms on the phase diagram are concave.

DOI: [10.1103/PhysRevB.98.060303](https://doi.org/10.1103/PhysRevB.98.060303)

Introduction. Temperature is a key statistical parameter associated with physical systems that can be characterized by statistical mechanics methods. Somewhat unexpectedly, such are nonlinear systems with evolution dynamics dictated by the ubiquitous discrete nonlinear Schrödinger equation (DNLSE). Rasmussen *et al.* have identified a thermalization zone on the phase diagram of DNLSE-governed systems in which regular statistical mechanics methods apply [1]. In the thermalization zone, self-trapping of energy does not occur and breathers are not formed. Rather, in a nonequilibrated system, a process of energy exchange starts, very slow at high nonlinearities, until system equilibrium is reached with statistics that can be described by the equipartition function. This thermalization zone is bounded by zero and infinite temperature lines, as shown in Fig. 1. A system placed at a specific point within the thermalization zone, as determined by the initial excitation conditions, will reach a statistical equilibrium with a unique temperature.

In this work we derive the system temperature between the zero and infinite temperature lines, and generate a map of temperatures in the strong nonlinearity (or strong interaction) limit. We have divided the thermalization zone into a *cold* zone and a *hot* zone and calculated entropies vs energy to derive temperatures across the thermalization zone.

The general notion of temperature of DNLSE systems has previously been applied in various studies: diffusion and nonequilibrium [2–5], instabilities [6], phase transitions [7–9], breather evolution [10–13], equation solution [14], trapped ultracold atoms [Bose-Einstein condensate (BEC)] [10,15–20], dynamics at low temperatures [21], Bloch oscillations [22], beam steering [23], and waves localization [24]. Our temperature expressions can therefore be useful to the study and unification of a wide range of physical systems. Franzosi derived an expression for temperatures in the microcanonical picture given systems with two first integrals [25]. Our study uses the common grand canonical picture.

Equation and conserved quantities. The fields’ evolution dynamics considered here is described by a normalized one-dimensional (1D) periodic cubic [14] DNLSE [26]:

$$i \frac{dU_m(z)}{dz} = -[U_{m-1}(z) + U_{m+1}(z)] - \Gamma |U_m(z)|^2 U_m(z). \quad (1)$$

Here U_m is the complex field at site m at position (or time) z . The array consists of N sites, assumed large, and periodic boundary conditions are employed.

Correlations of two fields separated by k sites are defined as

$$C_k(z) = \frac{1}{2N} \sum_{m=1}^N [U_m^*(z)U_{m+k}(z) + U_m(z)U_{m+k}^*(z)]. \quad (2)$$

To express energy quantities we apply the canonical transformation and write the complex field U_m as a product of an amplitude u_m (a real non-negative number) and a phase factor, $\exp(i\phi_m)$, and define an angle difference θ_m : $U_m \equiv u_m e^{i\phi_m}$; $I_m \equiv U_m U_m^* = u_m^2$; $\theta_m \equiv \phi_m - \phi_{m+1}$. We refer to I_m as site densities (with dimensions of energy).

The DNLSE [Eq. (1)] is nonintegrable [27,28], and has two constants of motion [14,29,30]. The first is the Hamiltonian \mathcal{h}_a , the sum of two unconserved quantities: $\mathcal{h}_a = \mathcal{h}_2(z) + \mathcal{h}_4(z)$ with

$$\begin{aligned} \mathcal{h}_2(z) &= \frac{2}{N} \sum_{m=1}^N u_m(z)u_{m+1}(z) \cos[\theta_m(z)] = 2C_1(z), \\ \mathcal{h}_4(z) &= \frac{\Gamma}{2} \frac{1}{N} \sum_{m=1}^N u_m^4(z). \end{aligned} \quad (3)$$

Here $\mathcal{h}_2(z)$ is the “kinetic energy,” and $\mathcal{h}_4(z)$ the “interaction energy.” The Hamiltonian \mathcal{h}_a as defined above is site-averaged. The second conserved quantity, $w_a = \frac{1}{N} \sum_{m=1}^N I_m(z)$, is the site-averaged density (or “norm” [2,26] or “wave action” [31]).

*uri.levy@weizmann.ac.il

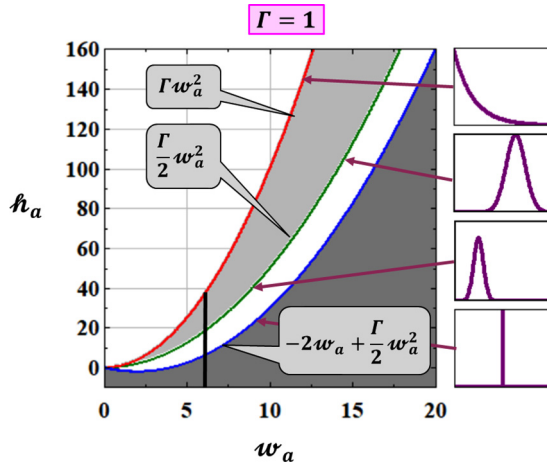


FIG. 1. Zones on the DNLSE phase diagram. The zone between the T_0 line (blue) and the T_∞ line (red) is the thermalization zone [1]. The thermalization zone is further divided by the L_i line (green) into a “cold zone” (white) and a “hot zone” (light gray). In the present work we limit the discussion mostly to systems with strong nonlinearity ($\Gamma w_a \gg 1$, that is, broadly to the right of the black vertical line at $w_a = 6$). The curves on the right are schematic representatives of PDF curves for the densities for each line.

Zones of the DNLSE phase diagram. The DNLSE phase diagram $\mathcal{h}_a(w_a)$ (see Fig. 1) can be divided into three zones: a lower *inaccessible zone*, a central *thermalization zone*, and an upper *negative temperature zone* [1]. The thermalization zone can be further divided into two: a lower *cold zone* and an upper *hot zone*. To be more specific, three limiting lines are defined as follows: zero temperature line (T_0 line): $\mathcal{h}_a(w_a) = -\text{sgn}(\Gamma)2w_a + (1/2)\Gamma w_a^2$, an intermediate line (L_i line): $\mathcal{h}_a(w_a) = (1/2)\Gamma w_a^2$, and an infinite temperature line (T_∞ line): $\mathcal{h}_a(w_a) = \Gamma w_a^2$. The intermediate L_i line is unique in terms of excitation. To place a system on this line it can be excited by equal amplitudes and fully random phases [32]. To place a system above this line, excitation amplitudes must be unequal. To place a system below this line, excitation phases cannot be fully random. The L_i line also has a physical meaning: it becomes the upper border of the thermalization zone for $\Gamma \rightarrow 0$ and it becomes the lower border of the thermalization zone for $\Gamma \rightarrow \infty$. Below we show that system temperature along most of the L_i line is $T(w_a) \cong 2w_a/|\Gamma|$.

Definition of temperatures in the strong nonlinearity limit. According to the quantum phase model, the entropy of DNLSE systems splits in the strong nonlinearity limit into a sum of entropies $s_\theta + s_I$ [32,33]. We define the DNLSE system temperature in the standard way (cf. the definition in [34]), with a small modification,

$$T_{\text{DNLSE}}(w_a, \mathcal{h}_a) = \left(\Gamma \frac{\partial s_{\text{sys}}(w_a, \mathcal{h}_a)}{\partial \mathcal{h}_a} \right)_{w_a}^{-1}, \quad (4)$$

where $s_{\text{sys}} = s_\theta + s_I$ and

$$s_\theta \equiv - \int_0^{2\pi} \mathcal{P}_\theta(\theta) \ln [\mathcal{P}_\theta(\theta)] d\theta, \quad (5)$$

$$s_I \equiv - \int_0^\infty \mathcal{P}_I(I) \ln [h \mathcal{P}_I(I)] dI; \quad h = 1.$$

$\mathcal{P}_\theta(\theta)$ and $\mathcal{P}_I(I)$ are equilibrium probability distribution functions (PDFs) for the relative angles (θ_m) or densities (I_m) across all sites of the large array. The value of the scale parameter h , with units of *energy*, is set at 1.

The entropy s_I of Eq. (5) is given by the Gibbs entropy equation [35], independent of the nonlinearity coefficient Γ . But in the microcanonical picture, the number of states of a DNLSE system grows exponentially with Γ (ignoring the typically small kinetic-energy contribution), and thus the entropy grows linearly with Γ . Here we keep the entropy dimensionless and insert the nonlinearity coefficient Γ into the temperature definition [Eq. (4)]. The dimension of DNLSE system temperature is thus *energy*². Indeed, as discussed below and as was verified by our ample numerical simulations across the high nonlinearity region of the DNLSE phase diagram, temperature is essentially equal to the density “variance,” also with units of *energy*². [If the PDF(I) is written as $\mathcal{P}_I(I) \propto \exp[-(a/2)I^2 - bI]$, then the density variance is $1/a$]. Clearly, much like the relations of temperature and the actual variance of *velocity* of gas molecules – low temperature \leftrightarrow narrow $\mathcal{P}_v(v)$ or $\mathcal{P}_I(I)$, high temperature \leftrightarrow wide $\mathcal{P}_v(v)$ or $\mathcal{P}_I(I)$.

Temperature calculation procedure. In the following sections we derive expressions for the DNLSE system temperatures, based on Eqs. (4) and (5). For that we need to find the entropy, and therefore the equilibrium PDFs for I and θ for each point on the phase diagram (w_a, \mathcal{h}_a). We found it convenient to start by assuming particular excitation conditions that equilibrate to different regions of the phase diagrams, and from these to calculate the resulting PDFs. With two specific excitation profiles we are able to cover the entire thermalization zone.

We show below that either exactly or to a very good approximation, the temperatures are given by the variance (σ_I^2) of the equilibrium PDF of density $\mathcal{P}_I(I)$. Since the variance is determined once the two parameters defining the equilibrium $\mathcal{P}_I(I)$ are determined, the temperature can be evaluated without calculating entropy and its derivative.

Equilibrium temperatures of systems in the cold zone. In this section we first derive analytic expressions for two equilibrium PDFs (density and phase-angle difference) and then, given these PDFs, derive the temperatures. We note that at zero temperature the system is in its ground state. The ground state is characterized by uniform amplitudes and zero ($\Gamma < 0$) or π ($\Gamma > 0$) relative phase between neighbors. At the ground state, regardless of system density, the variance of the density vanishes, $\sigma_I^2 = 0$.

(i) *PDF expressions for the cold zone.* A convenient statistical excitation to place a system in the cold zone is to excite all amplitudes uniformly with a value u_0 and select the phase angles randomly from a limited window of width ϕ_0 . For $\Gamma < 0$ the phase window is set around 0 for all sites. For $\Gamma > 0$ the phase window is set around 0 for odd sites and around π for even sites. A zero-width window ($\phi_0 = 0$) corresponds to excitation of the ground state. Broadening the phase window ϕ_0 from 0 to 2π will translate the system vertically on the phase diagram along a $w_a = u_0^2$ line from the T_0 line up to the L_i line.

By maximize system entropy (similar maximization is described in more detail in [36]) we have derived the following

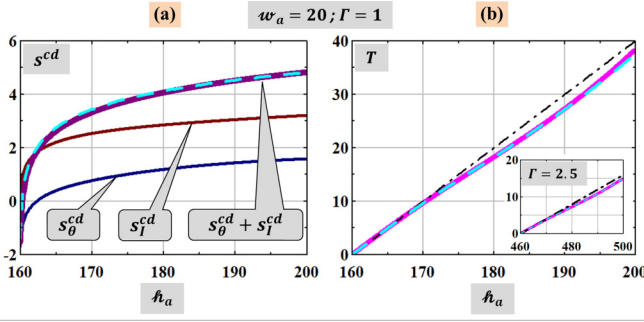


FIG. 2. System entropy and system temperature in the cold zone, for a fixed system density $w_a = 20$. (a) System entropy as the sum $s_{\text{sys}} = s_{\theta}^{cd} + s_I^{cd}$. The fitted curve (light dashed cyan) is a log curve. (b) System temperature. Magenta curve: calculated through Eqs. (5) and (4). Dashed-dotted straight line: the derivative of the fitted log curve of entropy. The dashed cyan line in Fig. 2(b) is given by the variance of $\mathcal{P}_I^{cd}(I)$, showing excellent match to the exact temperature. Inset: temperature in the cold zone for the higher nonlinearity coefficient ($\Gamma = 2.5$). The curve indicates that as the value of the nonlinearity coefficient ($\Gamma > 0$) increases, while the area of the entire cold zone shrinks relative to the total area of the thermalization zone, the slope of the line of system temperatures in the cold zone decreases.

PDF expressions (superscript “cd” stands for “cold”):

$$\begin{aligned} \mathcal{P}_I^{cd}(I) &= \frac{1}{\mathfrak{N}_I} e^{-(\eta\Gamma/2)(I-w_a)^2}, \\ \mathfrak{N}_I &= \sqrt{\frac{\pi}{2\eta\Gamma}} \left[1 + \operatorname{erf}\left(w_a \sqrt{\frac{\eta\Gamma}{2}}\right) \right], \\ \mathcal{P}_{\theta}^{cd}(\theta) &= \frac{1}{2\pi I_0(2\eta w_a)} e^{-[2\eta w_a \cos(\theta)]}, \end{aligned} \quad (6)$$

where $I_0(\cdot)$ is the modified Bessel function of the first kind. The parameter η is defined by

$$\begin{aligned} \eta \left\{ 4w_a \left[\int_0^{2\pi} \cos(\theta) \mathcal{P}_{\theta}(\theta) d\theta + C_0 \right] \right\} + 1 &= 0, \\ C_0 &= (1 - \cos \phi_0) / (0.5\phi_0^2), \\ \operatorname{sgn}(\eta) &= \operatorname{sgn}(\Gamma). \end{aligned} \quad (7)$$

The PDFs of Eq. (6) are determined by only one parameter, $\phi_0(w_a, \mathcal{h}_a)$. System energy is related to this one parameter by the monotonically rising function: $\mathcal{h}_a(\phi_0) = 2w_a C_0(\phi_0) + 0.5\Gamma w_a^2$. Inverting this equation (numerically) yields $\phi_0(w_a, \mathcal{h}_a)$.

(ii) *Equilibrium temperatures in the cold zone.* Given the expressions $\mathcal{P}_{\theta}^{cd}(\theta)$ and $\mathcal{P}_I^{cd}(I)$ from Eq. (6), entropies (s_{θ}^{cd} , s_I^{cd}) are calculated via Eq. (5) and temperatures are derived using Eq. (4). Entropy curves and temperature curves are shown in Figs. 2(a) and 2(b), respectively. The dash-dotted line of Fig. 2(b) is given by the variance of $\mathcal{P}_I^{cd}(I)$, that is, $T_{cd}(w_a, \mathcal{h}_a) = 1/(\eta\Gamma)$, showing an excellent match to the exact temperature, represented by the continuous magenta line.

The sum of entropies curve can be well approximated by a logarithmic function of the form $s_{\text{sys}}(w_a, \mathcal{h}_a) = \ln[\mathcal{h}_a - C_1(w_a)] + C_2$, as shown by the dashed line in Fig. 2(a).

The derivative of this log-fitted curve results in a particularly simple dependence of system temperature on the coordinates in the cold zone:

$$\begin{aligned} T_{cd}(w_a, \mathcal{h}_a) &\cong \frac{\mathcal{h}_a - C_1(w_a)}{\Gamma}, \\ C_1(w_a) &\equiv -\operatorname{sgn}(\Gamma)2w_a + \frac{1}{2}\Gamma w_a^2. \end{aligned} \quad (8)$$

For a fixed system density w_a , $T_{cd}(w_a, \mathcal{h}_a)$ of Eq. (8) grows linearly with energy: as system energy \mathcal{h}_a is increased from the T_0 line to the L_i line, the system temperature rises from zero to $2w_a/|\Gamma|$. This linear approximation is particularly good at low temperatures, and is shown by the dash-dotted line in Fig. 2(b).

Equilibrium temperatures of systems in the hot zone. To calculate temperatures in the hot zone, we assume a different excitation statistic, with fully random phases and a non-negative Gaussian distribution of amplitudes [34],

$$P(u > 0) = \frac{1}{\mathcal{R}_u} \exp\left[-\frac{(u - \mu)^2}{2\sigma^2}\right] \quad (9)$$

with \mathcal{R}_u appropriate normalization constant.

We have previously derived analytic equilibrium PDF expressions for such excitations. The lower part of the hot zone is still characterized by strong correlations between the sites, and we deal with it first. At higher temperatures, correlations are weak and simpler analysis can be employed.

(i) *Temperatures in the strong correlations region.* On and just above the L_i line, the strong field correlations characterizing systems in the cold zone persist [32,36]. Therefore, for systems placed in this region the kinetic-energy term [$\mathcal{h}_2(z_s) = 2C_1(z_s)$] cannot be neglected and must be included in the formulation of the temperature. As in the cold zone, both angle-associated entropy s_{θ}^{sc} , and density-associated entropy s_I^{sc} contribute, and the system’s entropy in the strong correlations region is given by the sum $s^{sc} = s_{\theta}^{sc} + s_I^{sc}$ [32,36]. Expressions for the PDFs in this strong correlation region, $\mathcal{P}_I^{sc}(I)$ and $\mathcal{P}_{\theta}^{sc}(\theta)$, were derived [[36], Eq. (16)]. These are given in terms of the two excitation parameters (μ, σ) through the statistical excitation moments, [$M_1(\mu, \sigma)$, $M_2(\mu, \sigma)$, $M_4(\mu, \sigma)$] [[36], Eq. (12)]. The conserved quantities are related to the excitation moments as $w_a(\mu, \sigma) = M_2(\mu, \sigma)$ and $\mathcal{h}_a(\mu, \sigma) = 0.5\Gamma M_4(\mu, \sigma)$. To determine (μ, σ), one needs to invert these two relations for [$M_2(\mu, \sigma)$, $M_4(\mu, \sigma)$], and solve for (μ, σ) and for $\eta_{sc}(M_1, M_2, M_3)$ [[36], Eq. (16)]. With those PDFs we can calculate the related entropies and the related temperature, $T_{sc}(w_a, \mathcal{h}_a)$.

(ii) *Temperatures in the weak correlations zone.* For points above the L_i line and toward the T_{∞} line, the interaction energy dominates. Under the weak correlation approximation (or “weak-coupling limit” [31]) the small kinetic-energy term ($\mathcal{h}_2 = 2C_1$) can be neglected and the PDF for the intensity becomes [31] -

$$\mathcal{P}_I^{wc}(I) = \frac{1}{\mathcal{R}_I} e^{-\epsilon I^2 - \alpha I}; \quad \epsilon \geq 0 \quad (10)$$

with \mathcal{R}_I an appropriate normalization constant. The two parameters $\epsilon(w_a, \mathcal{h}_a)$ and $\alpha(w_a, \mathcal{h}_a)$ are fixed such that the two conserved quantities (w_a, \mathcal{h}_a) are given by the first and second moments of this distribution.

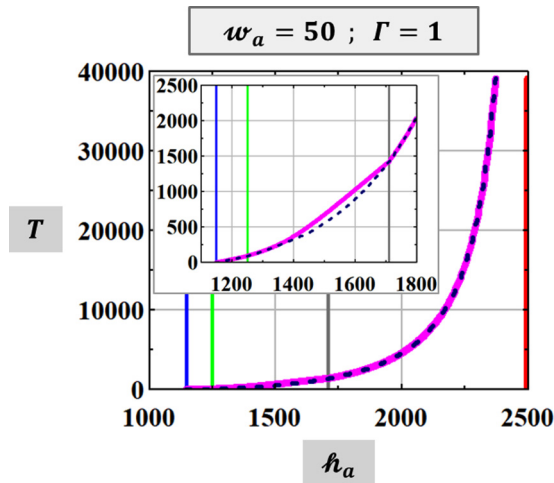


FIG. 3. A representative curve of temperatures of DNLSE systems at fixed system density ($w_a = 50$). The inset is a zoom-in to low system-energy values. The blue-green-red vertical markers mark the crossing of the (T_0 , L_i , T_∞) lines. The vertical gray line marks the position of switching from strong correlations to weak correlations in the hot zone as applied to temperature calculations. The dashed line is the variance of the density distribution (see text) that provides an excellent approximation to the temperature over most of the energy range.

The associated entropy is worked out to be $s_{wc}(w_a, \hbar_a) = \ln[\pi \mathcal{R}_I(w_a, \hbar_a)] + \frac{2\epsilon(w_a, \hbar_a)\hbar_a}{\Gamma} + \alpha(w_a, \hbar_a)w_a$. It turns out that only one term contributes to the temperature, leading to

$$T_{wc}(w_a, \hbar_a) = \left(\Gamma \frac{\partial s_{wc}(w_a, \hbar_a)}{\partial \hbar_a} \right)_{w_a}^{-1} = \frac{1}{2\epsilon(w_a, \hbar_a)}. \quad (11)$$

Note the difference by a factor of 2 compared with the temperature in Ref. [11]. We see from Eq. (11) that the temperature in the weak correlations zone of the DNLSE phase diagram is independent of the nonlinearity coefficient Γ . Further, the temperature in the weak correlations zone of the DNLSE phase diagram coincides with the variance $[1/2\epsilon(w_a, \hbar_a)]$ of the grand canonical Gaussian distribution of equilibrium densities $\mathcal{P}_I^{wc}(I)$. Here and in the text below we use variance to stand for the variance of a given PDF ($I \geq 0$) as if calculated for $-\infty < I < \infty$ and a renormalized PDF.

The two temperature curves $T_{sc}(w_a = C, \hbar_a)$ and $T_{wc}(w_a = C, \hbar_a)$ cross. The overall temperature curve for the hot zone is obtained by switching from $T_{sc}(w_a = C, \hbar_a)$ to $T_{wc}(w_a = C, \hbar_a)$ at their crossing point.

Equilibrium temperatures of systems on the DNLSE phase diagram. Figure 3 shows the overall curve of temperatures from the T_0 line to the T_∞ line (for a fixed system density). It is obtained by switching from derivation through $\mathcal{P}_\theta^{cd}(\theta)$ and $\mathcal{P}_I^{cd}(I)$ between the blue and the green markers, to derivation through $\mathcal{P}_\theta^{sc}(\theta)$ and $\mathcal{P}_I^{sc}(I)$ between the green and the gray markers, to derivation through $\mathcal{P}_I^{wc}(I)$ from the gray marker and on. The result is a single continuous curve as shown in Fig. 3. The dotted line shows the variance of the density PDF, which provides a good approximation for the temperature over most of the range. A full map of temperatures calculated for

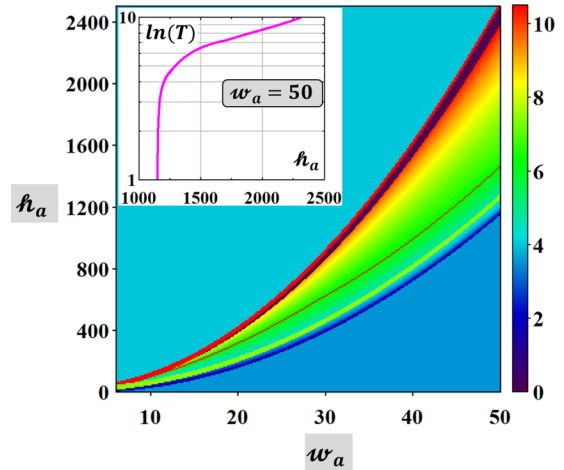


FIG. 4. Equilibrium temperatures of systems in the strong nonlinearity zone of the DNLSE phase diagram (note the \log_e scale of the map. Values below 1 were numerically raised to 1). Blue, green, and red lines are (T_0 , L_i , T_∞) lines, respectively. The region below the T_0 line is inaccessible, and the one above the T_∞ line is the negative temperatures region. The black area next to the T_∞ line represents very high yet not numerically calculated temperatures. The dark line crossing the map is a constant temperature line ($T = 500$). The inset shows a curve of temperatures (on a \log_e scale) vs system energy for a constant system density at the right edge of the map ($w_a = 50$; cf. Fig. 3). The curve shows very fast temperature rise getting closer to the T_∞ line.

the strong nonlinearity zone of the DNLSE phase diagram is shown by Fig. 4.

Discussion and conclusion. We have seen that excitations of the DNLSE system, depending on their initial values of density and energy, thermalize to particular equilibrium states. There is a set of nonstatistical excitations that seems to violate this thermalization claim. Namely, the set of eigenmodes of the linear system. These are characterized by equal amplitudes, equally spaced phases, and uniformly modified propagation wave numbers $\{U_{m,q}(z) = u_0 \exp[(i(m-1)\alpha_q)] \exp(ik_{zq}z); \alpha_q \equiv q2\pi/N; k_{zq} = 2 \cos \alpha_q + \Gamma u_0^2; q = -N/2, \dots, 0, \dots, N/2 - 1\}$. Mathematically, field amplitudes of these excitations will remain unaltered, thus corresponding to a zero temperature. However, these modes are unstable. If small noise is added (either amplitude noise or phase noise), the perturbed modes will thermalize according to their position in the thermalization zone.

We have demonstrated that the variance of the PDF of the density provides an excellent approximation for the temperature. As can be observed in Fig. 3, the only region where this approximation is less accurate is the transition region between strong and weak correlations in the hot zone, a region where our entropy-based derivation and PDFs are less exact. Note that the variance is the true variance of the PDF in the lower range of temperature, but broader than the actual variance in the high-temperature region, where the variance is calculated as if negative values for the density were allowed.

Our temperature analysis holds for both signs of the nonlinearity coefficient (Γ). In the temperature definition given by Eq. (4) both Γ and $\partial \hbar_a$ appear. Now, it is clear from the definition of the phase diagram, that if Γ changes signs,

the entire diagram flips through the horizontal mirror line of $\hbar_a = 0$, i.e., $\hbar_a \rightarrow -\hbar_a$. Thus, as both Γ and $\partial \hbar_a$ change signs simultaneously, temperatures remain positive and their values are independent of the nonlinearity sign. Note also that the temperature-related I^2 coefficients ($\eta\Gamma$) or α in the $\mathcal{P}_I(I)$ expressions are always positive, independent of the nonlinearity sign. Note that flip of the nonlinearity sign will *not* in general place a system on an equivalent point of the flipped phase diagram.

These results hold for all 1D nonlinear systems of equal sites that evolve under the DNLS dynamics: optical waveguides,

polymer chains, etc., including systems of trapped ultracold atoms that evolve under the dynamics of the equivalent Gross Pitaevskii equation, and they can be easily extended to higher-dimensional systems.

Acknowledgments. We are thankful to Oren Raz for many fruitful discussions. This work was supported by DIP - German-Israeli Project Cooperation, by a grant from the United States-Israel Binational Science Foundation (BSF), Jerusalem, Israel, and the United States National Science Foundation (NSF), by Icore - Israeli Centre of Research Excellence “Circle of Light”, and by the Crown Photonics Center.

-
- [1] K. Ø. Rasmussen, T. Cretegny, P. G. Kevrekidis, and Niels Grønbech-Jensen, *Phys. Rev. Lett.* **84**, 3740 (2000).
- [2] S. Iubini, S. Lepri, and A. Politi, *Phys. Rev. E* **86**, 011108 (2012).
- [3] A. Eisner and B. Turkington, *Phys. D (Amsterdam, Neth.)* **213**, 85 (2006).
- [4] S. Lepri, <http://www2.yukawa.kyoto-u.ac.jp/~ykis2015/ws/Presentation/Lepri.pdf>, 2015.
- [5] D. M. Basko, *Phys. Rev. E* **89**, 022921 (2014).
- [6] B. Rumpf and A. C. Newell, *Phys. Rev. Lett.* **87**, 054102 (2001).
- [7] E. Small, R. Pugatch, and Y. Silberberg, *Phys. Rev. A* **83**, 013806 (2011). See also the Supplemental Material cited within.
- [8] G. Situ, S. Muenzel, and J. W. Fleischer, [arXiv:1304.6980](https://arxiv.org/abs/1304.6980).
- [9] P. Buonsante, R. Franzosi, and A. Smerzi, *Phys. Rev. E* **95**, 052135 (2017).
- [10] P. G. Kevrekidis, *The Discrete Nonlinear Schrödinger Equation: Mathematical Analysis, Numerical Computations and Physical Perspectives* (Springer Science & Business Media, Berlin, 2009), Vol. 232.
- [11] B. Rumpf, *Phys. D (Amsterdam, Neth.)* **238**, 2067 (2009).
- [12] A. Trombettoni and A. Smerzi, *Phys. Rev. Lett.* **86**, 2353 (2001).
- [13] H. Hennig, T. Neff, and R. Fleischmann, *Phys. Rev. E* **93**, 032219 (2016).
- [14] S. Chatterjee and K. Kirkpatrick, *Commun. Pure Appl. Math.* **65**, 727 (2012).
- [15] A. Polkovnikov, S. Sachdev, and S. M. Girvin, *Phys. Rev. A* **66**, 053607 (2002).
- [16] V. S. Bagnato, D. J. Frantzeskakis, P. G. Kevrekidis, B. A. Malomed, and D. Mihalache, *Rom. Rep. Phys.* **67**, 5 (2015).
- [17] E. H. Lieb, R. Seiringer, J. P. Solovej, and J. Yngvason, *The Mathematics of the Bose Gas and its Condensation* (Springer Science & Business Media, Berlin, 2005), Vol. 34.
- [18] A. Smerzi, S. Fantoni, S. Giovanazzi, and S. R. Shenoy, *Phys. Rev. Lett.* **79**, 4950 (1997).
- [19] S. Raghavan, A. Smerzi, S. Fantoni, and S. R. Shenoy, *Phys. Rev. A* **59**, 620 (1999).
- [20] J. Choi, S. Hild, J. Zeiher, P. Schauß, A. Rubio-Abadal, T. Yefsah, V. Khemani, D. A. Huse, I. Bloch, and C. Gross, *Science* **352**, 1547 (2016).
- [21] C. B. Mendl and H. Spohn, *J. Stat. Mech.* (2015) P08028.
- [22] S. Droulias, Y. Lahini, Y. Kominis, P. Papagiannis, Y. Bromberg, K. Hizanidis, and Y. Silberberg, *New J. Phys.* **15**, 093038 (2013).
- [23] D. N. Christodoulides, F. Lederer, and Y. Silberberg, *Nature (London)* **424**, 817 (2003).
- [24] S. Flach, *Nonlinear Dynamics: Materials, Theory and Experiments* (Springer, Cham, 2016), pp. 45–57.
- [25] R. Franzosi, *J. Stat. Phys.* **143**, 824 (2011).
- [26] J. C. Eilbeck and M. Johansson, in *Localization and Energy Transfer in Nonlinear Systems*, edited by L. Vázquez, R. S. MacKay, and M. P. Zorzano (World Scientific, Singapore, 2003), pp. 44–67.
- [27] M. J. Ablowitz and B. Prinari, in *Encyclopedia of Mathematical Physics*, edited by J. P. Francoise, G. L. Naber, and S. T. Tsou (Elsevier, Amsterdam, 2006), Vol. 5, p. 552.
- [28] N. Finlayson and K. J. Blow, *Chaos, Solitons Fractals* **4**, 1817 (1994).
- [29] A. K. Sarma, M. A. Miri, Z. H. Musslimani, and D. N. Christodoulides, *Phys. Rev. E* **89**, 052918 (2014).
- [30] N. Korabel and G. M. Zaslavsky, *Phys. A (Amsterdam, Neth.)* **378**, 223 (2007).
- [31] B. Rumpf, *Phys. Rev. E* **77**, 036606 (2008).
- [32] Y. Silberberg, Y. Lahini, Y. Bromberg, E. Small, and R. Morandotti, *Phys. Rev. Lett.* **102**, 233904 (2009).
- [33] S. D. Huber, B. Theiler, E. Altman, and G. Blatter, *Phys. Rev. Lett.* **100**, 050404 (2008).
- [34] C. Kittel and H. Kroemer, *Thermal Physics* (W.H. Freeman and Company, New York, 2000).
- [35] M. E. Popović, *Thermal Sci.* **22**, 1163 (2018).
- [36] U. Levy, K. Yang, N. Matzliah, and Y. Silberberg, *J. Phys. B: At., Mol. Opt. Phys.* **51**, 035401 (2018).